

JGR Space Physics

RESEARCH ARTICLE

10.1029/2019JA026630

Key Points:

- The stability of KH billows in the MLT region on Reynold number and Prandtl number on long-lasting “C-type” structure in the Na lidargram
- Low temperature can increase magnitude of Prandtl number and convectively stable atmosphere can decrease the magnitude of Reynolds number
- This conducive atmosphere is responsible for the long lifetime of the remnant of previously generated KH billows in the MLT region

Correspondence to:

S. Sarkhel,
sarkhel.fph@iitr.ac.in

Citation:

Mondal, S., Sarkhel, S., Agarwal, J., Chakrabarty, D., Sekar, R., Yuan, T., et al. (2019). On the long lasting “C-type” structures in the sodium lidargram: The lifetime of Kelvin-Helmholtz billows in the mesosphere and lower thermosphere region. *Journal of Geophysical Research: Space Physics*, 124, 3110–3124. <https://doi.org/10.1029/2019JA026630>










Received 21 FEB 2019

Accepted 7 APR 2019

Accepted article online 13 APR 2019

Published online 30 APR 2019

On the Long Lasting “C-Type” Structures in the Sodium Lidargram: The Lifetime of Kelvin-Helmholtz Billows in the Mesosphere and Lower Thermosphere Region

S. Mondal¹ , S. Sarkhel¹ , Jay Agarwal¹, D. Chakrabarty² , R. Sekar² , Tao Yuan³ , Xuguang Cai³ , Alan Z. Liu⁴ , Satonori Nozawa⁵ , Norihito Saito⁶, Takuya D. Kawahara⁷, Martin G. Mlynczak⁸ , and James M. Russell III⁹

¹Department of Physics, Indian Institute of Technology Roorkee, Roorkee, India, ²Space and Atmospheric Sciences Division, Physical Research Laboratory, Ahmedabad, India, ³Physics Department, Utah State University, Logan, UT, USA, ⁴Center for Space and Atmospheric Research & Department of Physical Sciences, Embry-Riddle Aeronautical University, Daytona Beach, FL, USA, ⁵Institute for Space-Earth Environmental Research (ISEE), Nagoya University, Nagoya, Japan, ⁶Photonics Control Technology Team, RIKEN Center for Advanced Photonics, Wako, Japan, ⁷Faculty of Engineering, Shinshu University, Nagano, Japan, ⁸Atmospheric Sciences Division, NASA Langley Research Center, Hampton, VA, USA, ⁹Center for Atmospheric Sciences, Hampton University, Hampton, VA, USA

Abstract In order to understand the characteristics of long-lasting “C-type” structure in the Sodium (Na) lidargram, six cases from different observational locations have been analyzed. The Na lidargram, collected from low-, middle-, and high-latitude sites, show long lifetime of the C-type structures which is believed to be the manifestation of Kelvin-Helmholtz (KH) billows in the Mesosphere and Lower Thermosphere (MLT) region. In order to explore the characteristics of the long-lasting C-type structures, the altitude profile of square of Brunt-Väisälä frequency in the MLT region has been derived using the temperature profile collected from the Na lidar instruments and the SABER instrument onboard TIMED satellite. It is found to be positive in the C-type structure region for all the six cases which indicates that the regions are convectively stable. Simultaneous wind measurements, which allowed us to calculate the Richardson numbers and Reynolds numbers for three cases, suggest that the regions where the C-type structure appeared were dynamically stable and nonturbulent. This paper brings out a hypothesis wherein the low temperature can increase the magnitude of the Prandtl number and convectively stable atmospheric region can cause the magnitude of Reynolds number to decrease. As a consequence, the remnant of previously generated KH billows in nearly “frozen-in” condition can be advected through this conducive region to a different location by the background wind where they can sustain for a long time without much deformation. These long-lived KH billows in the MLT region will eventually manifest the long-lasting C-type structures in the Na lidargram.

1. Introduction

The existence of layers of neutral metal atoms and its ions was first detected by sunlight’s resonant scattering (Slipher, 1929). The formation of these layers in the Mesosphere and Lower Thermosphere (MLT) region (80 to 110 km) is due to the ablation of meteors. Development of lidar in early 1960s (Bowman et al., 1969) has helped in detailed study of vertical distributions of these metal atoms and its ions. Sodium (Na) is the easiest among all the metals which present in the atmospheric layer to measure because of its large resonant scattering cross section. There are occurrences of sporadic thin layers of enhanced concentration of metals, which were first reported for Na then subsequently for other metals, superposed over the regular background layers and are called sporadic neutral (Ns) layers (e.g., Clemesha et al., 1978). Neutralization of metal ions concentrated by wind shear mechanism in the lower *E* region is given as a possible explanation for formation of Ns layers (Axford, 1967). The lidar measurements of the neutral Na atoms concentration over low- and high-latitude stations have been carried out for several decades (e.g., Clemesha et al., 1979; Clemesha, 2004; Collins et al., 2002; Sarkhel, Raizada, et al., 2012, 2019; Sarkhel et al., 2009, 2010; Takahashi et al., 2014; Tsuda et al., 2011, 2015). Na lidar observations from Arecibo Observatory (Kane et al., 2001) revealed the occurrence of a different type of sporadic Na layer, which was very different in appearance from normal Ns layers and occurred much less frequently. Kane et al. (2001) interpreted these layers as related to field aligned ionospheric irregularities. Normal Ns layers do not show any kind of

rapid temporal variations with height, and they appear as quasi horizontal structures in lidargram (Clemesha et al., 1999). However, different layers reported by Kane et al. (2001) and Raizada et al. (2015) show complex structure in the lidargram, which somewhat resembled overturning structures. They lasted for around an hour and extended for several kilometers vertically. It was suggested that these complex structures could be the indication of prominent dynamics features, such as Kelvin-Helmholtz (KH) instabilities in regions of strong wind shear.

The ripple-type structures frequently observed in airglow images within the same region by several researchers (e.g., Cai et al., 2014; Hecht et al., 1997, 2000; Peterson, 1979; Taylor & Hill, 1991; Taylor & Hapgood, 1990; Taylor et al., 1997) are the indication of instabilities in the layers. Hecht et al. (1997, 2000, 2001) have shown that both large wind shears and super adiabatic lapse rate were the cause of these structures. KH instability can lead to form KH billows structures in a dynamically unstable region due to a large wind shear, and the onset condition of formation of billow can be judged by the Richardson number (Ri) (Richardson, 1920), which is the ratio of static stability and square of wind shear. Whenever it is less than its canonical threshold value (0.25), it causes the atmosphere to become dynamically unstable and KH billows may form in that region (e.g., Gossard & Hooke, 1975; Miles & Howard, 1964). The dynamical instability may be created if the wind shear is sufficiently large, and it plays a critical role in the neutral Na layer. Pfrommer et al. (2009) observed KH billows using a high-resolution Na lidar in the MLT region which is due to the dynamic instability which also responsible for generating various short-period structures in the MLT region (e.g., Sarkhel, Sekar, et al., 2012). In order to study the evolution and the lifetime of these structures, many theoretical and observational studies have been carried out (Browning & Watkins, 1970; Browning, 1971; Davis & Peltier, 1979; Klaassen & Peltier, 1985a, 1985b, 1991; Thorpe 1968, 1973) including 3-D simulations to provide more realistic scenario of the evolution of KH billows and secondary instabilities (Caulfield & Peltier, 1994; Caulfield & Peltier, 2000; Fritts et al., 1996; Palmer et al., 1994, 1996; Peltier & Caulfield, 2003; Werne & Fritts, 1999). Based on the laboratory experiments, Thorpe (1968, 1973) suggested, as the evolution of KH billows takes place, secondary instabilities are formed which eventually decay into turbulence.

Clemesha et al. (2004) reported several similar cases, similar to Kane et al. (2001), and have alternately explained the formation of complex structures which is commonly referred as “C-type” structures. The structure appeared in the sodium lidargram looks like “C” alphabet with overturning feature. They suggested that these structures could be resultant or remnant of spatial structures advected over the lidar site rather than wave breaking or KH instabilities as suggested by Kane et al. (2001) because of limited correlation found between sporadic *E* layers and these structures. Larsen et al. (2004) also reported similar type of structure with ~1- to 3-hr timescale. They discussed about the possible physical processes behind the generation of this type structure and concluded to be convective instability instead of KH instability. Sridharan et al. (2009) also reported four such cases over Gadanki, India, which occurred in early morning. The observations carried out by them are in complete agreement with the suggestions reported by Kane et al. (2001) that the strong wind shear was present during all the four cases. Therefore, Sridharan et al. (2009) supported the hypothesis, proposed by Kane et al. (2001), of KH instability for the formation of complex sporadic structures. Sarkhel et al. (2015a, 2015b) have examined the Na lidargram from Gadanki, India, on a night using a meteor radar from Thiruvananthapuram, India, and satellite borne measurements. They suggested that the KH billow formation took place over Thiruvananthapuram, southern part of India. The wind measurements suggest that the billow was initially modified due to the wind shear. Then, it eventually got “frozen-in” the background due to the reduction of vertical wind shear and was advected to the lidar site. They concluded that the lifetime of KH billows could be of order of a few hours, under favorable background conditions, in the MLT region. Therefore, those long lasting KH billow manifests as a long lasting C-type structure in the Na lidargram. The question that remained unaddressed was what kind of background conditions can enable KH billows to survive hours together in apparently frozen-in condition.

In this paper, we will analyze six cases from low-, middle-, and high-latitude locations, wherein C-type structures have been detected by lidar system on the Na lidargram. Based on this study, we will attempt to conclude the dependency of lifetime of KH billows on different atmospheric parameters and finding the background condition for which KH billow can last longer in the MLT region and appear as long lasting C-type structure in the Na lidargram.

Table 1

The First Three Cases of the “C-Type” Structure (Cases 1–3) With the Date of the Events, Occurrence Time Duration Including the References, and the Vertical Extent of Those Structure

Case no.	Date of the event	Location of the site	References	C-type occurrence time (in UTC)	Altitude region of C-type structure
1	27 Nov 2005	Gadanki (13.5 °N, 79.2 °E)	Sridharan et al. (2009)	17:00–18:00	94–98 km
2	18 Mar 2007	Gadanki (13.5 °N, 79.2 °E)	Sarkhel et al. (2015a)	16:00–16:30	93–98 km
3	13 May 2013	Hefei (31 °N, 117.0 °E)	Qiu et al. (2018)	16:55–19:13	92–98 km

2. Experimental Techniques

In order to assess the effect of different atmospheric parameters on the occurrence of the C-type structures appeared in the Na lidargram, we have chosen six cases from low-, middle-, and high-latitude sites where the C-type structure is observed clearly in the Na lidargram. The details of the sites and the occurrence of the C-type structures are given in Tables 1 and 3. The altitude profiles of temperature for the first three cases (Table 1) have been obtained from the SABER (Sounding of Atmosphere using Broadband Emission Radiometry) instrument onboard TIMED (Thermosphere Ionosphere Mesosphere Energetics and Dynamics) satellite (data source: <http://saber.gats-inc.com>; v2.0; Level 2A). SABER uses the 15- μm terrestrial emission from CO_2 molecules to retrieve pressure at a given altitude, which is then utilized to derive the altitude profile of temperature. The altitude profile of uncertainty in deriving the temperature from SABER in the altitude range of 80–105 km is available in Mertens et al. (2001). SABER measurement locations and time chosen nearest to the observing sites (Gadanki, India, and Hefei, China) are given in Table 2. Altitude profile of temperature and wind data for last three case have been measured from the resonance Na lidar. It provides high-resolution spatial and temporal data compared to the SABER data set. It is also capable of simultaneous measurements of mesospheric temperature profile and horizontal wind profiles along with neutral Na density. The details on the resonance Na lidar system over Gadanki, derivation of Na density measurement, and its statistical error are given in Bhavani Kumar et al. (2007). The description of the Na lidar over Tromsø, Norway, is available in Nozawa et al. (2014) and Kawahara et al. (2017).

3. Data Analysis

The dynamic instability of the atmosphere is characterized by the Richardson number (Richardson, 1920). It is defined as follows:

$$Ri(z) = \frac{N^2(z)}{S^2(z)} \quad (1)$$

where N^2 is the square of Brunt-Väisälä frequency which follows the equation:

$$N^2(z) = \frac{g}{T(z)} \left[\frac{g}{C_p} + \frac{dT(z)}{dz} \right] \quad (2)$$

where $T(z)$ is temperature at height z (meter), C_p is the molecular specific heat at constant pressure (1,004 J kg^{-1} K^{-1} for diatomic molecules like N_2 and O_2), g is the acceleration due to gravity ($g \approx 9.8 \text{ m/s}^2$), and S^2 is the square of resultant vertical shear, which is defined as follows:

$$S^2(z) = \left(\frac{du}{dz} \right)^2 + \left(\frac{dv}{dz} \right)^2 \quad (3)$$

where u and v are the altitude profile of zonal and meridional wind, respectively. The dynamical instability occurs when $Ri < 0.25$ and $N^2 < 0$ suggest the occurrence of convective instability in the medium. The temperature profiles for the three cases listed in Table 1 are obtained from the SABER instrument onboard TIMED satellite. In order to get the optimized temperature profile, the satellite measurement locations have been chosen in nearest proximity to the Na lidar sites and closest to the time of the event when the C-type structure appeared in the Na lidargram (shown in Tables 1 and 2). As reported in Kishore Kumar et al. (2008), the average temporal variation in the nocturnal temperature over Gadanki (a low-latitude station)

Table 2

The Location and the Measurement Time (in UTC) of the SABER Instrument Onboard TIMED Satellite Near to the Location Site of the Cases Mentioned in Table 1

Case No.	Date of satellite measurement	Time of satellite measurement (HH:MM:SS)	Satellite measurement location	Average temperature (K) of the C-type altitude region	Prandtl number
1	27 Nov 2005	18:16:03	12.23 °N, 82.38 °E	172	0.75
2	18 Mar 2007	19:59:32	13.56 °N, 86.71 °E	183	0.74
3	13 May 2013	13:55:58	30.25 °N, 107.50 °E	174	0.75

Note. The average temperature and the corresponding Prandtl number of the air in the region of “C-type” structures for those cases.

is not significant in the altitude range of 80–105 km. Therefore, the satellite-retrieved temperature profile, measured a few hours before or after the event occurred, is valid enough and will not alter our conclusions. Since Hefei, China, is also a geographically low-latitude station, the same argument can also be drawn for this site. Therefore, the simultaneous measurements of wind, temperature, and Na atom density profiles are available for the last three cases (shown in Figures 2–4).

In order to assess the stability of C-type structures in MLT region, the magnitude of the Prandtl (Pr) number of the air medium is calculated in the region. Pr is defined as the ratio of momentum diffusivity (kinematic viscosity) to thermal diffusivity:

$$Pr = \frac{\nu}{\alpha}$$

where ν is kinematic viscosity and α is the *thermal diffusivity* which is defined as

$$\alpha = \frac{k}{C_p \rho}$$

Hence, we have the expression for the Prandtl number

$$Pr = \frac{C_p \mu}{k}$$

where C_p is specific heat capacity at constant pressure, ρ is the density of air medium, μ is dynamic viscosity ($\nu \cdot \rho$), and k is the thermal conductivity of the air medium.

Following Zografos et al. (1987), an empirical expression for the Prandtl number in case of air at the temperature (T) in Kelvin (K) (T is the average temperature taken in the altitude region where C-type structures appeared) can be written as follows:

$$Pr = 1.0677 \times 10^{-23} T^7 - 7.6511 \times 10^{-20} T^6 + 1.0395 \times 10^{-16} T^5 + 4.6851 \times 10^{-13} T^4 - 1.7698 \times 10^{-9} T^3 + 2.2260 \times 10^{-6} T^2 - 1.1262 \times 10^{-3} T + 0.8835 \quad (4)$$

It is to be noted that this expression is valid for range of temperature 100–3,000 K at 1 atm pressure. It is a well-known fact that the pressure is very low in the MLT region, and therefore, air gas can be considered behaving as an ideal gas (Çengel & Boles, 2015). In case of an ideal gas, C_p , μ , and k are independent of air pressure, and thus, Prandtl number, which depends on the magnitudes of C_p , μ , and k , is independent of pressure in the MLT region (Çengel & Cimbala, 2017). Hence, the effect of pressure while deriving the Prandtl number in MLT region has already been taken care. Therefore, in practice, the equation (4) will give significant accuracy in deriving Prandtl number of air medium in the MLT region. The maximum uncertainty for deriving Prandtl number within the regions of C-type structures is 0.01. It is interesting to note that the Prandtl number of air medium within the Tropospheric Boundary Layer (TBL) is ~ 0.7 .

4. Results

The left column of Figure 1 depicts the temperature profiles obtained from SABER instrument onboard TIMED satellite for all the first three cases nearest to the observational sites (details shown in Table 2),

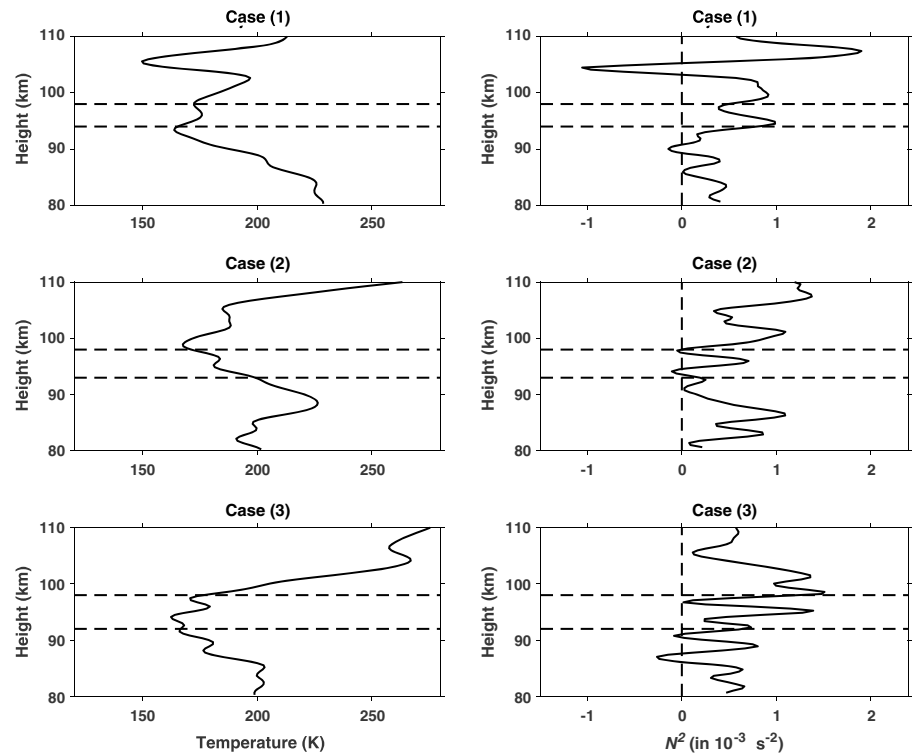


Figure 1. The temperature profiles obtained from SABER (left column) and the corresponding Brunt-Väisälä frequency square (N^2) profiles (right column) for all the three cases shown in Tables 1 and 2. The horizontal dotted line in every case is the altitude range in where the “C-type” structure appeared in the Na lidargram, and vertical dotted line on the Right column represents Brunt-Väisälä frequency of “Zero” magnitude.

whereas the right column represents the square of Brunt-Väisälä frequency (N^2) obtained from the SABER temperature profile using the equation (2). The horizontal dashed lines in every case indicate the altitude range where the unusual C-type structure appeared in the Na lidargram. The vertical dashed lines on the right column of the Figure 1 indicate zero value of N^2 . The right column shows that the values of N^2 for all the three cases (given in Table 1) in the altitude range wherein the C-type structure appeared to be positive. In case (2), the magnitude of N^2 becomes slightly negative ($-0.105 \times 10^{-3} \text{ s}^{-2}$ at 94 km and $-0.049 \times 10^{-3} \text{ s}^{-2}$ at 97.5-km altitude). However, the maximum uncertainty in N^2 (ΔN^2) within the region of the C-type structure is $0.114 \times 10^{-3} \text{ s}^{-2}$. Hence, we cannot draw any conclusion that the N^2 is negative for case (2) in the region of the C-type structure. Overall, the temperature structure indicates that those regions were *convectively stable* at the time of C-type structure appearance for those corresponding cases (time and locations of the respective observational sites are given in Tables 1 and 2).

Figure 2 presents the Na lidar measurements over Cerro Pachón, Chile (30.3 °S, 70.7 °W; low-latitude site) on 30 October 2017. Figures 2a–2f, respectively, depict the height-time map of neutral Na atom density (Na lidargram), temperature, N^2 (from equation (2)), zonal wind, meridional wind, and Ri number (from equation (1)). Similarly, Figures 3 and 4, respectively, present the Na lidar measurements over Logan, USA (42 °N, 112 °W), on 31 July 2013 and Tromsø, Norway (66.9 °N, 19.2 °E), on 14 December 2014. From Figure 2a, the Na lidargram shows the C-type structure appeared during 2:00–4:00 UTC in the altitude range of 97 to 103 km over Cerro Pachón, Chile. The C-type structure over this site occurs during 9:30–10:00 UTC in the lidargram over Logan, USA (Figure 3a). Figure 4a shows the C-type structures in the Na lidargram over Tromsø, Norway, that appears during 22:00–26:00 UTC within the altitude range of 90–99 km. The C-type structures are clearly visible in the Na lidargram for these three cases, and the other details of those events are tabulated in Table 3. The average occurrence time of all the C-type events, tabulated in Tables 1 and 3, is found to be in the range of 30 min to a few hours and the vertical extent of those structures is in the range of 4–10 km. The N^2 is found to be positive in the region of C-type structure for all the six cases which

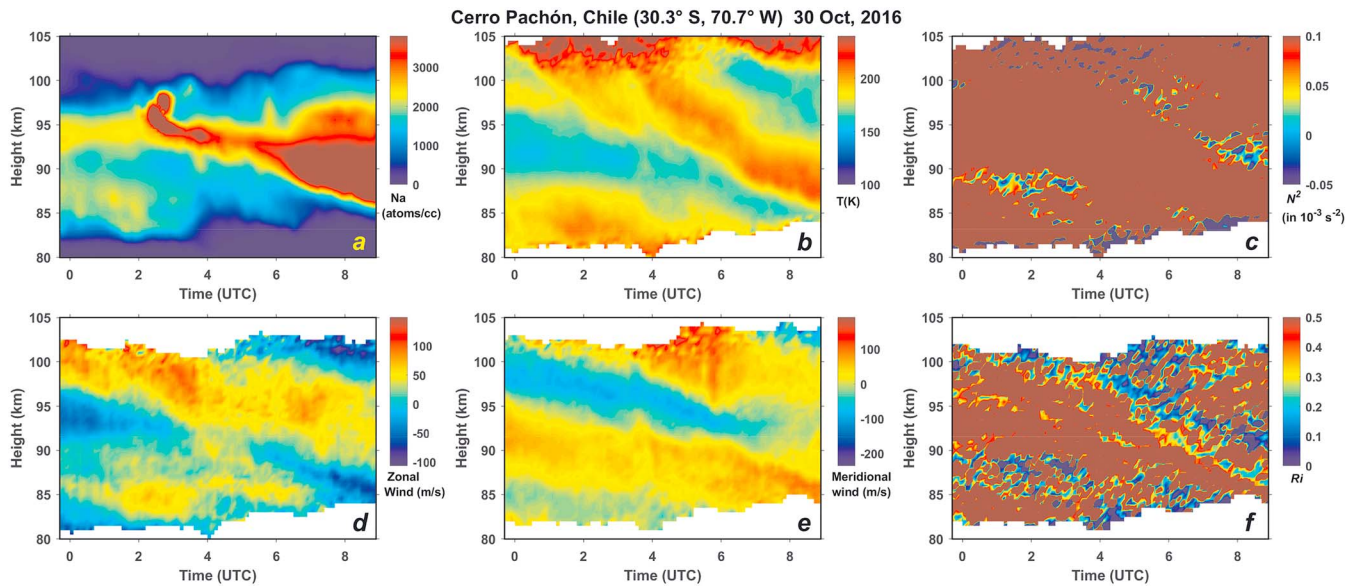


Figure 2. (a–c) Na lidargram, absolute temperature (in K), and the square of Brunt-Väisälä frequency (N^2) over Cerro Pachón, Chile (low latitude), on 30 October 2016, respectively. (d–f) The map of zonal wind, meridional wind, and derived Richardson number.

implies the region was convectively stable. The maps of Ri for the last three cases (shown in Figures 2f, 3f, and 4f) found to always greater than the threshold limit 0.25 in the region of C-type structure indicating that nonexistence of dynamical instability. The Prandtl numbers calculated in the altitude region of C-type structures are more than 0.7 for the all six cases (shown in Tables 2 and 3). The Reynolds numbers, calculated for the last three cases, are found be less than 1,000 (shown in Table 3) which is the clear indication of nonturbulent medium.

5. Discussion

It is well-known that the Na lidar records horizontally-narrow vertical profiles of Na atom concentration as a function of time. Thus, the height-time-concentration map of neutral Na atoms or the “lidargram”

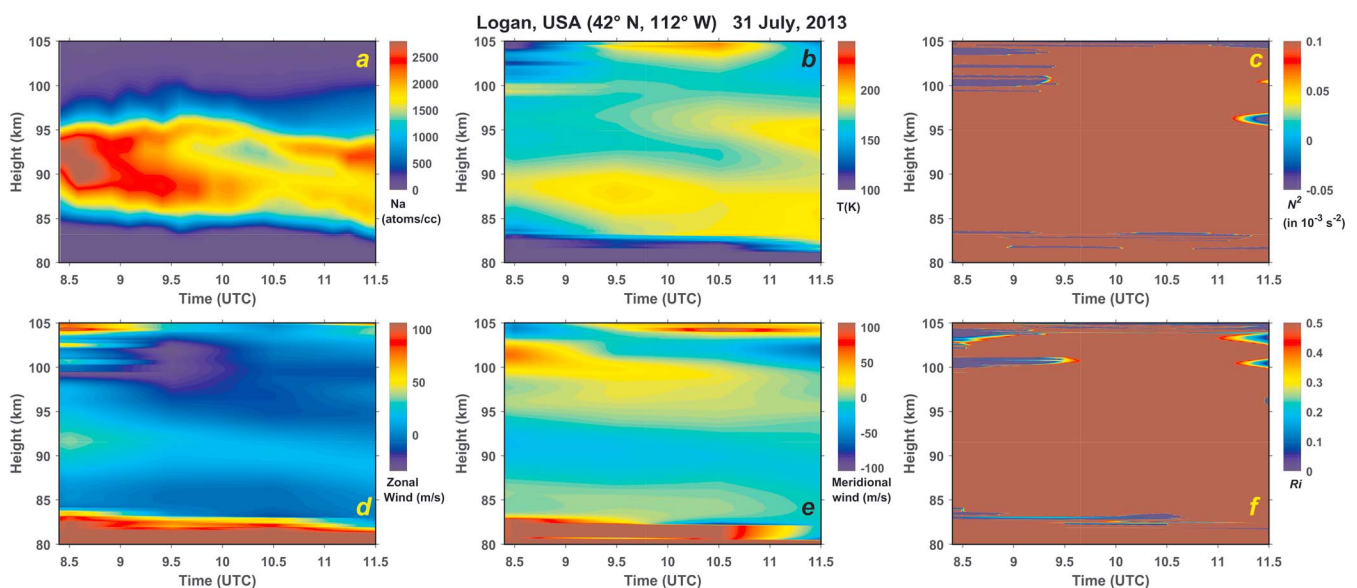


Figure 3. (a–c) Na lidargram, absolute temperature (in K), and the square of Brunt-Väisälä frequency (N^2) over Logan, USA (mid latitude), on 31 July 2013, respectively. (d–f) The map of zonal wind, meridional wind, and derived Richardson number.

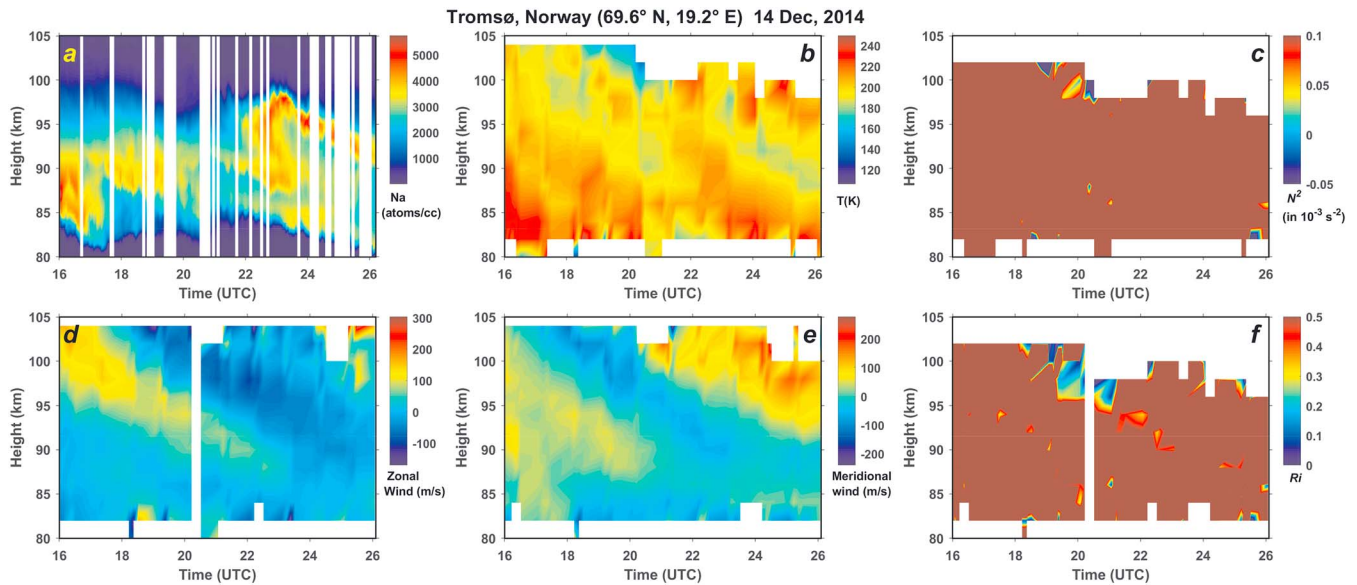


Figure 4. (a–c) Na lidargram, absolute temperature (in K), and the square of Brunt-Väisälä frequency (N^2) over Tromsø, Norway (high latitude), on 14 December 2014, respectively. (d–f) The map of zonal wind, meridional wind, and derived Richardson number.

represents a time history of the vertical distribution of Na atoms in a narrow cylindrical volume over the lidar location. As the neutral Na atoms in the layer have a long chemical lifetime relative to the evolution of atmospheric dynamics (Xu & Smith, 2003), they are collisionally well embedded in the neutral atmosphere. The C-type structures observed in the lidargram on several occasions could be caused by wave breaking or KH billows and may be generated in the Na layer due to strong wind shear (Kane et al., 2001). As described in Sarkhel et al. (2015a), a KH billow structure can imprint a C-type structure in the lidargram. Therefore, in order to judge the persistence of the C-type in the lidargram, the evolution of KH billows needs to be investigated.

The features of KH billow or instability have been observed for decades (e.g., Browning, 1971; Hecht et al., 1997, 2000; Peterson, 1979; Taylor & Hapgood, 1990; Taylor et al., 1997; Taylor & Hill, 1991). As earlier referred, the atmosphere becomes conducive for the generation of KH billows and dynamically unstable, whenever Ri becomes less than the canonical threshold, 0.25. The evolution of these KH billows depends on a few atmospheric parameters that will decide its evolution and lifetime. These are discussed below:

5.1. Role of Viscosity: Reynolds Number (Re)

For homogenous fluid, if we consider the viscosity term, then the energy lost from mean flow in creating the fluid particle deformation will not be available for feeding any kind of instabilities. Therefore, there should

Table 3
Date, Locations, and Time (in UTC) of the Events Mentioned in Figures 2–4

Date and location of event	C-type occurrence time (in UTC)	Altitude range of C-type structure	Average temperature (K) of the C-type altitude region	Prandtl number (Pr)	Reynolds Number (Re)
30 Oct 2016 Cerro Pachón, Chile (30.3 °S, 70.7 °W)	02:00–04:00	93–99 km	184	0.74	146
13 Jul 2013 Logan, USA (40.6 °N, 105 °W)	09:30–10:00	86–96 km	181	0.74	245
14 Dec 2014 Tromsø, Norway (69.6 °N, 19.2 °E)	22:00–26:00	90–99 km	199	0.73	641

Note. Average temperature in the region of interest (“C-type” structure) and obtained magnitudes of the Prandtl numbers and the Reynolds numbers for those cases.

be a *stabilizing* effect on shear flow dynamics due to introduction of viscosity term. We can estimate the magnitude of this stabilizing effect using molecular Reynolds number (Re) with the following relation:

$$Re = \frac{u \cdot h}{\nu} \quad (5)$$

where h is taken as the half depth of the unstable layer, u is half of the velocity difference across unstable layer, and ν being kinematic viscosity (Hecht et al., 2005). Re is the comparison of maximum available mean kinetic energy with the linear damping per unit mass, which is contributed by the production of stress, that is, comparison of viscous and inertial forces. Therefore, the relationship between the mean shear and the wave instability becomes more complex due to presence of this viscosity term. The importance of the effect of Re on the lifetime and evolution of KH billow is described in the next subsections.

5.2. Dependence of the Lifetime of KH Billows on Re From Different Models

Klaassen and Peltier (1985a, 1985b, 1991) have suggested a model (known as *KP model*), wherein Ri is variable and Re is in between 300 and 900. The initial billow formation takes slightly longer time which is around 3.5 to 7 min. When Re is 500, secondary instability occurs at around 9 min. At around 11 min, the secondary instability's maximum growth rate was achieved. Moreover, at 13 min, it had maximum amplitude at an amplification factor of 20 to 30% of the primary KH billow. When Re has magnitude of 300, the secondary instabilities have much lower growth rates. For Re of 500, the lifetime is around 20 min. Similar to FP model, the KP model also suggests that whenever the magnitude of Re is higher, the lifetime of the KH billow is reduced.

Palmer et al. (1996) and Fritts et al. (1996) have suggested a model (known as *FP model*), which has Re as 0.05 and Re as 300 and 500, that reach maximum amplitude after 8 min from starting and billows collapse into turbulence after around 12 min. However, when Re is 300, the turbulence is over by around 25 min. The collapse of billow is slower than for Re of 500 cases, wherein collapsing structures were much coherent and less turbulent as compared to Re of 500. Thus, the lifetime of KH billow for Re of 300 is more compared to Re with 500, which can be estimated around 25 min.

Hill et al. (1999) and Werne and Fritts (1999) discussed a model (known as *HW model*) with Ri of 0.05 and Re as 2,000, in which billow growth is maximum at around 10 min. Between 14 and 18 min, the secondary instabilities become visible. The structures collapsed after 29 min which implies that the lifetime of the secondary instability is around 10 min, as observed by Palmer et al. (1996) and Fritts et al. (1996), (FP model) when Re was 500.

Caulfield and Peltier (2000) have discussed a model which has the magnitude of Ri between 0 and 0.125 and Re of 750. The lifetime of KH billow is around 20–30 min. The above studies suggest that the decrease in the Re generally leads to the increase in the lifetime of the KH billows. Also, according to Hecht et al. (2005), the KH billows in mesopause region appeared to last longer than those observed in the troposphere based on observations by Browning and Watkins (1970) and Browning (1971), which had lifetime of less than 15 min in the troposphere.

5.3. Effect of Prandtl Number on the Evaluation of KH Billow

In the fluid mechanics, the Prandtl number (Pr) is defined as: $Pr = \nu/\alpha$, where ν is the kinematic viscosity of the fluid and α is the thermal diffusivity. By definition, it is clear that unlike Re , it contains no such length scale and depends only on the fluid state. Therefore, it is a property of the fluid itself not the flow state. The growth and collapse of the KH billow are common features in a stably stratified shear flow and play a crucial part in the dynamics and energetics of the upper atmosphere. Numerous numerical analyses and laboratory experiments have been carried out to understand the nonlinear evaluation of KH billow with various Prandtl numbers (e.g., Klaassen & Peltier, 1985a; Peltier & Caulfield, 2003; Thorpe, 2005). However, the dependence of Prandtl number on the evaluation of KH billow, which appeared in the upper atmosphere, is not well understood. In order to assess the stability of KH billow in a density-stratified fluid, we are trying to study the evolution of KH billow in conjunction with the Prandtl number. The objective is to find out the dependency of KH billow on the Prandtl number and its influence on the characteristics of KH billow. The Prandtl number may have numerous effects on energy budget of KH billow and the exchange of energy of that with

the mean flow energy. On basis of the previous numerical and laboratory experiment, the variation of the amplitude and stability of billow structures with the Prandtl number are briefly described below.

This section is dedicated to understand whether the Prandtl number plays any role to the variation of vertical scale height of C-type structure which is believed as the manifestation of the KH billow in Na lidargram. One of the most characteristic features of KH instability is the variation of vertical scale height of KH billows. Klaassen and Peltier (1985c) observed that the density stratification has a stabilizing effect on the formation of KH billow, and consequently, the shear flow having greater thermal diffusion rate (which means lower Prandtl number) should lead to form KH billows with maximum vertical scale height. The numerical study by Rahmani et al. (2016) also confirmed that the KH billows with lower Prandtl number achieve larger vertical extent. Thereafter, lower Prandtl number shear flow might be the reason of the higher vertical extends of the KH billow in the MLT region. The vertical extent of KH billows in a flow having lower Prandtl number ($Pr \sim 0.7$) medium is found to be in the range of a few kilometers, whereas the vertical range of KH billows in the Ocean with higher Prandtl number ($Pr \sim 13.6$) is about a few meters (De Silva et al., 1996). Larsen et al. (2004) also reported overturning or roll type structure on the Na lidargram, similar to C-type in the MLT region. They also found nearly 5- to 6-km vertical extents of those overturning or rolls type structure. In this context, our results tabulated in the Tables 2 and 3 reveal few kilometer vertical extents for all the observed locations. Therefore, there is a correlation between the vertical extent of KH billow and the Prandtl number. It indicates that the lower Prandtl number leads to the higher vertical extent of KH billow or the C-type structure.

5.4. Effect of Convective and Dynamic Stability: Brunt-Väisälä Frequency and Richardson Number

Thermal or convective stability and dynamics stability play important role in upper atmosphere whether the frozen-in condition of KH billow will last long and will depend on the thermal stability of the medium, which is controlled by temperature gradient. On the other hand, the dynamics stability of the medium is controlled by the wind shear. This section is devoted to study the thermal stability as well as the dynamical stability of the background condition in the region of C-type structure and the role of different atmospheric parameters to the convective and dynamical stability.

5.4.1. Convective Stability

It is a well-known fact that the thermal convection depends upon the temperature gradient. The thermal convection in the medium plays an important role in the mixing of the species present in the medium. This motivates us to investigate the altitude profiles of temperature gradient and, hence, Brunt-Väisälä frequency over the Na lidar locations to study the effect of thermal stability in the region of C-type structure.

In turbulent thermal convection, Prandtl number and Rayleigh number (Ra) are also imperative and control parameters. In this context, an asymptotic expression of Rayleigh number in Rayleigh-Bénard convection, which is useful to the present scenario, can be expressed as follows:

$$Ra \sim \frac{\beta \cdot g \cdot L^4 \cdot T'}{(\nu \cdot \alpha)} \quad (6)$$

where L is vertical scale size of the C-type structure, T' is the temperature gradient between the colder upper and warmer lower surfaces ($\frac{dT}{dx}$), g is the acceleration due to gravity, and β , ν , and α are, respectively, the thermal expansion coefficient, the kinematic viscosity, and the thermal diffusivity of the convecting fluid (Grossmann & Lohse, 2002; Qiu & Tong, 2001). The experimental observations suggest that the relationship between Ra , Re , and Pr is $Re \sim Ra^{0.43} Pr^{-0.76}$ (Lam et al., 2002). Therefore, Ra increases with the magnitude of the negative temperature gradient and subsequently increases the magnitude of Re that leads to the turbulent atmosphere in the mesosphere. In addition, it is clear from the equation (2) that if the magnitude of negative temperature gradient increases and more than the adiabatic lapse rate (g/C_p), square of Brunt-Väisälä frequency (N^2) becomes negative and the atmosphere becomes convectively unstable. Therefore, the relationship between Re and N^2 is consistent and conclusively indicates that the convectively stable atmosphere leads to lower magnitude of Ra and hence Re .

It is to be noted that the above relationship of Ra with Re and Pr from Lam et al. (2002) applies to thermal (Rayleigh-Bénard) convection, in which the fluid velocities develop from the temperature gradients.

Interestingly, Figures 2–4 depict the negligible wind shear during the observation of the C-type structure in the MLT region over low-, middle-, and high-latitude stations. Therefore, this is the condition wherein the thermal convection due to the temperature gradient will play dominant role in the stability of KH billow in the MLT region, and any existing KH billow structure will be affected primarily by the convection. This is the similar situation to Rayleigh-Bénard thermal convection, wherein fluid velocities developed solely due to the temperature gradients and the convective cell is generated in the medium. This type convective cell can also be generated in the MLT region due to the temperature gradient which can lead to the distortion of any existing structure in the medium (like C-type structure in the present case).

The Prandtl number plays an important role in the secondary instability. This secondary instability, which is convective in nature, has a crucial role in vertical mixing of fluids. Increasing Prandtl number has profound effects on small-scale features like secondary instability, which sometimes developed in the outer core of the billow. As discussed in the Data Analyses, the Prandtl number is the ratio of momentum diffusivity (kinematic viscosity) to thermal diffusivity. The momentum transfer is related to the kinematic viscosity while the diffusion of heat is related to the thermal diffusivity in the region of interest. In equation (4), it can be inferred that the Prandtl number is dependent on the temperature of the region of interest. It indicates that the increase in the temperature leads to the decrease in the magnitude of Prandtl number, which means higher thermal conductivity and/or lower viscosity of the region. This enables the heat transfer by thermal convection between the bottom warmer region and the upper cooler region of the KH billow in the mesosphere, activating the convective cells that tend to mix between the two regions. On the other hand, if the temperature is decreased, the Prandtl number is increased, which indicates low thermal conductivity and/or the region becomes more viscous. As discussed in Majumder et al. (2002), the fluid becomes stiffer and more time is required for the development of structure from an initial temperature perturbation. Hence, the thermal convective cell between the bottom and the upper region of the KH billow in the mesosphere will not be very effective. Therefore, the collapsing of billow will take a longer time in a fluid having higher Prandtl number. Rahmani et al. (2014) also indicated the extension of overall lifetime of the KH billow in high Prandtl number fluid.

5.4.2. Dynamic Stability

The dynamic stability is mainly controlled by the wind shear. Therefore, the medium with large wind shear or dynamically unstable region may not conducive for long lifetime of KH billow. It is earlier mentioned that the magnitude of Ri is the indication of dynamical instability of the atmosphere which occurs when $Ri < 0.25$. The maps of Richardson number for the last three cases found always greater than the threshold limit of 0.25 in the region of C-type structure indicating that nonexistence of dynamical instability. In addition, the Reynolds numbers, which are calculated for the last three cases, are found be less than 1,000 which is the clear indication of nonturbulent medium. Hence, the conclusion can be drawn that the KH billows that manifested as the C-type structures in the Na lidargram over Cerro Pachón, Chile, Logan, USA, and Tromsø, Norway, are not locally generated. Rather, they were generated earlier at some other locations and advected through a nonturbulent medium to reach the Na lidar site. The nonturbulent medium preserves the shape of any overturning structure which was previously generated in other locations due to strong wind shear. These are called frozen-in structures which are advected by the background wind without much deformation.

5.5. Lifetime of KH Billow

As discussed above, we can directly relate the turbulence with the magnitude of Re and Prandtl number wherein the turbulence will likely occur when the magnitude of Re is high and Prandtl number is low. In the present investigation, the Prandtl number derived for all the six cases (shown in Tables 2 and 3) from low-, middle-, and high-latitude stations is more than the typical magnitude of Prandtl number observed within the TBL. The Re , which is calculated for the last three cases, are found be less than 1,000 which is the clear indication of nonturbulent medium. It is also discussed that convectively stable atmosphere leads to lower magnitude of Re . Despite there are no wind measurements for the first three cases available with us, we can also extend the same argument that the magnitude of Re must have been in the lower side in that altitude region as it was convectively stable during the occurrence of the C-type structure in the Na lidargram over all those observational sites. In this connection, it is important to note that the observations of C-type structures from the different locations reveal that they lasted for 30 min to a few hours and bring

out the existence of KH billows in the Na layer. As discussed above, the C-type structure is the manifestation of a KH billow in the lidargram; hence, the lifetime of the KH billow must be somewhere in between 30 min and a few hours. The longer lifetime of the KH billow is because of the low magnitude of Re and increase in the magnitude of the Prandtl number in that altitude region. Tables 2 and 3 reveal that the Prandtl numbers for all the locations within the C-type structure region are noticeably greater than 0.7, which is the magnitude of the Prandtl number in the TBL. This is consistent with the observation reported by Hecht et al. (2005) that the KH billows in the MLT region appear to last longer than the KH billows observed in the troposphere using radar observation reported by Browning (1971) and Browning and Watkins (1970). However, the accurate estimation of the Prandtl number is very difficult in the MLT region. Experimental measurement of the eddy Prandtl number from photographic tracking of rocket released chemical clouds was found to be ~ 3 , but the data was significantly scattered (Justus, 1967). Several numerical studies also suggest that the effective value of eddy Prandtl number should be much greater than 1 in the MLT region (Coy & Fritts, 1988; Gavrilov & Yudin, 1992; Huang & Smith, 1991; Strobel et al., 1985, 1987; Strobel, 1989). Strobel et al. (1985), Strobel (1989), and Basseur and Solomon (2005) reported that the tracer and heat transport in the mesosphere can be best reproduced by taking Prandtl number ~ 3 . In this context, Strobel et al. (1987) also suggested a large value of the Prandtl number (~ 10) in the mesosphere after deriving eddy momentum diffusion coefficient from momentum stress, constituents transport, and heat transport (Johnson & Killeen, 1995). Thereby, experimental and numerical studies show that the effective value of the Prandtl number is much higher in the MLT region compared to the TBL region. As discussed above, the longer lifetime of KH billows is possible when the magnitude of the Prandtl number is increased. Hence, the lifetime of KH billows in the MLT region is expected to be longer than in TBL provided other parameters remained unaltered. In the present investigation, the magnitude of the Prandtl numbers for all the observed cases must have been very high, and as a result, the KH billow or the C-type structure lasted for longer time.

It is clear from the above discussion that the gradient of temperature and wind shear will dictate the overall lifetime of KH billows in the MLT region. The maps of Richardson number for the last three cases found always greater than the threshold limit 0.25 in the region of C-type structure indicating that it was not locally generated due to strong wind shear. Convectively and dynamically stable regions are conducive to sustain KH billows for a longer time once they are generated due to a strong wind shear. If the strong wind shear persists for a long time, the vertical mixing will prevent KH billows from persisting for a long time. However, if there is a significant reduction in the magnitude of a wind shear, the further evolution and deformation are ceased and the remnant of the previously generated KH billows can get nearly frozen-in the background. Qiu et al. (2016) also support the frozen-in concept. They observed the same C-type structure in Na lidargram from different lidar locations in China. The structure advected by the background wind without much deformation that was detected at different time by a series of Na lidars, although there is no scope in this present paper to determine the generation mechanism of KH billows or the similar bow-like shape structure as discussed by Clemesha et al. (2004). However, this present paper brings out the hypothesis wherein these previously generated KH billows in frozen-in condition can be advected by the background wind to a different location through the low temperature and convectively stable region where they can sustain for a long time without much deformation. These long-lived KH billows, in nearly frozen-in condition, will eventually manifest as the long-lasting C-type structures in the lidargram.

5.6. Limitation and Justification

The temperature profiles utilized to derive N^2 for the first three cases have been measured by the SABER instrument onboard the TIMED satellite. These satellite-retrieved temperature profiles from the SABER are less accurate compared to the temperature profiles measured by the Na lidar, used for last three cases. In addition, the time and measurement locations may not exactly coincide with the event and the lidar location, respectively. Moreover, there are also no wind data available for the first three cases. Therefore, there is no scope of calculating Ri and Re for the first three cases to assess the effect of dynamical instability and turbulence of the altitude region wherein C-type structures occurred over the Na lidar location. However, we have other three case studies from different latitude sites (low, middle, and high latitude) with simultaneous measurements of wind and temperature profiles, which are enough to validate the hypothesis. Hence, based on the adequate data set for the last three cases, we can also extend same argument for the first three cases that low temperature and convectively stable atmosphere in the MLT region can be conducive for

the longer lifetime of the already formed KH billows that are advected to the lidar location wherein they manifest as the long-lasting C-type structure in the Na lidargram.

6. Summary and Conclusion

The characteristics of the C-type structure appeared in the Na lidargram have been analyzed in order to investigate the evolution of the KH billow in the MLT region. The appearance of this unusual structure in the lidargram is independent of the locations and depends only on the physical processes. In order to validate the hypothesis, we have analyzed the Na lidargram for six cases from low-, middle-, and high-latitude locations. The lidar observations of neutral Na atoms concentration from these sites are complemented by the temperature measurements either by the same Na lidar or by the SABER instrument onboard TIMED satellite. Simultaneous wind measurements are also available for over Cerro Pachón, Chile, Logan, USA, and Tromsø, Norway. An attempt has been made to understand how the lifetime of the KH billow depends on the various atmospheric parameters in the MLT region: Reynolds number, Prandtl number, and Richardson number. The altitude profile of Brunt-Väisälä frequency (N^2) derived from the temperature measurement found to be positive for all the cases in the region of C-type structure. The height-time maps of Reynolds number clearly indicate the nonturbulent atmosphere over Cerro Pachón, Chile, Logan, USA, and Tromsø, Norway, during the event. It has been proven that the convectively stable atmosphere leads to the low Reynolds number and hence nonturbulent atmosphere. Based on the adequate data set for the last three cases, we can also extend same argument for the first three cases that the convectively stable atmosphere leads to the nonturbulent atmosphere. In addition, the Prandtl numbers for all the locations in the altitude region of C-type structure were found to be noticeably greater than the Prandtl number in TBL. The larger magnitude of Prandtl number is the indication that the thermal convective cell between the bottom and the upper region of the KH billow in the mesosphere will not be very effective. As a result, the collapsing of the billow will take a longer time that increases its lifetime. Moreover, the height-time maps of Richardson number for the last three cases found always greater than the threshold limit 0.25 in the region of C-type structure indicating that it was not locally generated due to strong wind shear. Based on the results obtained in this investigation, it has been finally concluded that the low temperature and convectively stable atmospheric in the MLT region will be the conducive medium wherein the remnant of previously generated KH billows can be advected in nearly frozen-in condition through this conducive region to a different location by the background wind where they can sustain for a long time without much deformation. These long-lived KH billows in the MLT region will eventually manifest the long-lasting C-type structures in the lidargram.

Acknowledgments

S. M. acknowledges the fellowship from the Ministry of Human Resource Development, Government of India for carrying out this research work. D. C. and R. S.'s components of this effort are supported by the Department of Space, Government of India. The Na lidar operation at Andes Lidar Observatory, Cerro Pachón, Chile, is supported by the grants AGS-1135278, 1734553, and 1759471 from National Science Foundation, USA. The Na lidar operation at Utah State University is supported by grant AGS-1135882 from National Science Foundation, USA. The Na lidar operation at Tromsø is partly supported by Grants-in-Aid for Scientific Research (17H02968) of Japan Society for the Promotion of Science (JSPS). The SABER temperature data is available from <http://saber.gats-inc.com> website. The Na lidar data at the Andes Lidar Observatory and Utah State University are available from the Madrigal site (<http://cedar.openmadrigal.org>). The Na lidar data at Tromsø is available from <http://www.isee.nagoya-u.ac.jp/~nozawa/indexlidardata.html> website. S. S. acknowledges David C. Fritts for his useful discussion on Reynolds number. This research work is also supported by the Ministry of Human Resource Development, Government of India.

References

- Axford, W. I. (1967). The wind shear theory of the formation of the temperate zone sporadic E layers. *Space Research*, 7, 126–133.
- Bhavani Kumar, Y., Rao, D. N., Murthy, M. S., & Krishnaiah, M. (2007). Resonance lidar system for mesospheric sodium measurements. *Optical Engineering*, 46(8), 086203. <https://doi.org/10.1117/1.2767271>
- Bowman, M. R., Gibson, A. J., & Sandford, M. C. W. (1969). Atmospheric sodium measured by a Tuned Laser Radar. *Nature*, 221(5179), 456–457. <https://doi.org/10.1038/221456a0>
- Brasseur, G., & Solomon, S. (2005). *Aeronomy of the middle stratosphere: Chemistry and physics of the stratosphere and mesosphere* (3th ed.). Dordrecht, Netherlands: Springer. <https://doi.org/10.1007/1-4020-3824-0>
- Browning, K. A. (1971). Structure of the atmosphere in the vicinity of large-amplitude Kelvin-Helmholtz billows. *Quarterly Journal of the Royal Meteorological Society*, 97(413), 283–299. <https://doi.org/10.1002/qj.49709741304>
- Browning, K. A., & Watkins, C. D. (1970). Observations of clear air turbulence by high power radar. *Nature*, 227(5255), 260–263. <https://doi.org/10.1038/227260a0>
- Cai, X., Yuan, T., Zhao, Y., Pautet, P.-D., Taylor, M. J., & Pendleton, W. R. (2014). A coordinated investigation of the gravity wave breaking and the associated dynamical instability by a Na lidar and an Advanced Mesosphere Temperature Mapper over Logan, UT (41.7°N, 111.8°W). *Journal of Geophysical Research: Space Physics*, 119, 6852–6864. <https://doi.org/10.1002/2014JA020131>
- Caulfield, C. P., & Peltier, W. R. (1994). Three dimensionalization of the stratified mixing layer. *Physics of Fluids*, 6(12), 3803–3805. <https://doi.org/10.1063/1.868370>
- Caulfield, C. P., & Peltier, W. R. (2000). The anatomy of the mixing transition in homogeneous and stratified free shear layers. *Journal of Fluid Mechanics*, 413, 1–47. <https://doi.org/10.1017/s0022112000008284>
- Cengel, Y. A., & Cimbala, J. M. (2017). *Fluid mechanics: Fundamentals and applications* (4th ed., p. 956). New York: McGraw-Hill Education.
- Çengel, Y. A., & Boles, M. A. (2015). *Thermodynamics: An engineering approach* (8th ed., p. 139). New York: McGraw-Hill Education.
- Clemesha, B. R. (2004). A review of recent MLT studies at low latitudes. *Annales Geophysicae*, 22(9), 3261–3275. <https://doi.org/10.5194/angeo-22-3261-2004>
- Clemesha, B. R., Batista, P. P., & Simonich, D. M. (1999). An evaluation of the evidence for ion recombination as a source of sporadic neutral layers in the lower thermosphere. *Advances in Space Research*, 24(5), 547–556. [https://doi.org/10.1016/S0273-1177\(99\)00199-4](https://doi.org/10.1016/S0273-1177(99)00199-4)

- Clemesha, B. R., Batista, P. P., Simonich, D. M., & Batista, I. S. (2004). Sporadic structures in the atmospheric sodium layer. *Journal of Geophysical Research*, *109*, D11306. <https://doi.org/10.1029/2003JD004496>
- Clemesha, B. R., Kirchhoff, V. W. J. H., Simonich, D. M., & Takahashi, H. (1978). Evidence of an extra-terrestrial source for the mesospheric sodium layer. *Geophysical Research Letters*, *5*(10), 873–876. <https://doi.org/10.1029/GL005i010p00873>
- Clemesha, B. R., Kirchhoff, V. W. J. H., Simonich, D. M., Takahashi, H., & Batista, P. P. (1979). Simultaneous observations of sodium density and the NaD, OH (8, 3), and OI 5577-Å, nightglow emissions. *Journal of Geophysical Research*, *84*(A11), 6477. <https://doi.org/10.1029/JA084ia11p06477>
- Collins, S. C., Plane, J. M. C., Kelley, M. C., Wright, T. G., Soldán, P., Kane, T. J., et al. (2002). A study of the role of ion-molecule chemistry in the formation of sporadic sodium layers. *Journal of Atmospheric and Solar-Terrestrial Physics*, *64*(7), 845–860. [https://doi.org/10.1016/s1364-6826\(02\)00129-3](https://doi.org/10.1016/s1364-6826(02)00129-3)
- Coy, L., & Fritts, D. C. (1988). Gravity wave heat fluxes: A Lagrangian approach. *Journal of the Atmospheric Sciences*, *45*, 1770–1780.
- Davis, P. A., & Peltier, W. R. (1979). Some characteristics of the Kelvin-Helmholtz and resonant overreflection modes of shear flow instability and of their interaction through vortex pairing. *Journal of the Atmospheric Sciences*, *36*(12), 2394–2412. [https://doi.org/10.1175/1520-0469\(1979\)036<2394:scotkh>2.0.co;2](https://doi.org/10.1175/1520-0469(1979)036<2394:scotkh>2.0.co;2)
- De Silva, I. P. D., Fernando, H. J. S., Eaton, F., & Hebert, D. (1996). Evolution of Kelvin-Helmholtz billows in nature and laboratory. *Earth and Planetary Science Letters*, *143*(1-4), 217–231. [https://doi.org/10.1016/0012-821x\(96\)00129-x](https://doi.org/10.1016/0012-821x(96)00129-x)
- Fritts, D. C., Palmer, T. L., Andreassen, Ø., & Lie, I. (1996). Evolution and breakdown of Kelvin-Helmholtz billows in stratified compressible flows. Part I: Comparison of two- and three-dimensional flows. *Journal of the Atmospheric Sciences*, *53*(22), 3173–3191. [https://doi.org/10.1175/1520-0469\(1996\)053<3173:eabokb>2.0.co;2](https://doi.org/10.1175/1520-0469(1996)053<3173:eabokb>2.0.co;2)
- Gavrilov, N. M., & Yudin, V. A. (1992). Model for coefficients of turbulence and effective Prandtl number produced by breaking gravity waves in the upper atmosphere. *Journal of Geophysical Research*, *97*(D7), 7619–7624. <https://doi.org/10.1029/92JD00185>
- Gossard, E. E., & Hooke, W. H. (1975). *Waves in the atmosphere, atmospheric infrasound and gravity waves: Their generation and propagation* (p. 456). New York: Elsevier Sci.
- Grossmann, S., & Lohse, D. (2002). Prandtl and Rayleigh number dependence of the Reynolds number in turbulent thermal convection. *Physical Review E*, *66*(1). <https://doi.org/10.1103/physreve.66.016305>
- Hecht, J. H., Fricke-Begemann, C., Walterscheid, R. L., & Höffner, J. (2000). Observations of the breakdown of an atmospheric gravity wave near the cold summer mesopause at 54°N. *Geophysical Research Letters*, *27*(6), 879–882. <https://doi.org/10.1029/1999GL010792>
- Hecht, J. H., Liu, A. Z., Walterscheid, R. L., & Rudy, R. J. (2005). Maui mesosphere and lower thermosphere (Maui MALT) observations of the evolution of Kelvin-Helmholtz billows formed near 86 km altitude. *Journal of Geophysical Research*, *110*, D09S10. <https://doi.org/10.1029/2003JD003908>
- Hecht, J. H., Walterscheid, R. L., Fritts, D. C., Isler, J. R., Senft, D. C., Gardner, C. S., & Franke, S. J. (1997). Wave breaking signatures in OH airglow and sodium densities and temperatures: 1. Airglow imaging, Na lidar, and MF radar observations. *Journal of Geophysical Research*, *102*(D6), 6655–6668. <https://doi.org/10.1029/96JD02619>
- Hecht, J. H., Walterscheid, R. L., & Vincent, R. A. (2001). Airglow observations of dynamical (wind shear-induced) instabilities over Adelaide, Australia, associated with atmospheric gravity waves. *Journal of Geophysical Research*, *106*(D22), 28,189–28,197. <https://doi.org/10.1029/2001JD000419>
- Hill, R. J., Gibson-Wilde, D. E., Werne, J. A., & Fritts, D. C. (1999). Turbulence-induced fluctuations in ionization and application to PMSE. *Earth, Planets and Space*, *51*(7-8), 499–513. <https://doi.org/10.1186/bf03353211>
- Huang, T. Y. W., & Smith, A. K. (1991). The mesospheric diabatic circulation and the parameterized thermal effect of gravity wave breaking on the circulation. *Journal of the Atmospheric Sciences*, *48*(8), 1093–1111. [https://doi.org/10.1175/1520-0469\(1991\)048<1093:tmdcat>2.0.co;2](https://doi.org/10.1175/1520-0469(1991)048<1093:tmdcat>2.0.co;2)
- Johnson, R. M., & Killeen, T. L. (1995). *The upper mesosphere and lower thermosphere: A review of experiment and theory* (Vol. 87). Washington, USA: American Geophysical Union.
- Justus, C. G. (1967). The eddy diffusivities, energy balance parameters and heating rates of upper atmospheric turbulence. *Journal of Geophysical Research*, *72*, 1035–1039.
- Kane, T., Grime, B., Franke, S., Kudeki, E., Urbina, J., Kelley, M., & Collins, S. (2001). Joint observations of sodium enhancements and field-aligned ionospheric irregularities. *Geophysical Research Letters*, *28*(7), 1375–1378. <https://doi.org/10.1029/2000GL012176>
- Kawahara, T. D., Nozawa, S., Saito, N., Kawabata, T., Tsuda, T. T., & Wada, S. (2017). Sodium temperature/wind lidar based on laser-diode-pumped Nd:YAG lasers deployed at Tromsø, Norway (696°N, 192°E). *Optics Express*, *25*(12), A491. <https://doi.org/10.1364/oe.25.00a491>
- Kishore Kumar, G., Venkat Ratnam, M., Patra, A. K., Vijaya Bhaskara Rao, S., & Russell, J. (2008). Mean thermal structure of the low-latitude middle atmosphere studied using Gadanki Rayleigh lidar, Rocket, and SABER/TIMED observations. *Journal of Geophysical Research*, *113*, D23106. <https://doi.org/10.1029/2008JD010511>
- Klaassen, G. P., & Peltier, W. R. (1985a). The evolution of finite amplitude Kelvin-Helmholtz billows in two spatial dimensions. *Journal of the Atmospheric Sciences*, *42*(12), 1321–1339. [https://doi.org/10.1175/1520-0469\(1985\)042<1321:eofakb>2.0.co;2](https://doi.org/10.1175/1520-0469(1985)042<1321:eofakb>2.0.co;2)
- Klaassen, G. P., & Peltier, W. R. (1985b). The onset of turbulence in finite amplitude Kelvin-Helmholtz billows. *Journal of Fluid Mechanics*, *155*, 1–35. <https://doi.org/10.1017/s0022112085001690>
- Klaassen, G. P., & Peltier, W. R. (1985c). The effect of Prandtl Number on the evolution and stability of Kelvin-Helmholtz billows. *Geophysical and Astrophysical Fluid Dynamics*, *32*(1), 23–60. <https://doi.org/10.1080/03091928508210082>
- Klaassen, G. P., & Peltier, W. R. (1991). The influence of stratification on secondary instability in free shear layers. *Journal of Fluid Mechanics*, *227*, 71–106. <https://doi.org/10.1017/s0022112091000046>
- Lam, S., Shang, X.-D., Zhou, S.-Q., & Xia, K.-Q. (2002). Prandtl number dependence of the viscous boundary layer and the Reynolds numbers in Rayleigh-Bénard convection. *Physical Review E*, *65*, 066306. <https://doi.org/10.1103/physreve.65.066306>
- Larsen, M. F., Liu, A. Z., Gardner, C. S., Kelley, M. C., Collins, S., Friedman, J., & Hecht, J. H. (2004). Observations of overturning in the upper mesosphere and lower thermosphere. *Journal of Geophysical Research*, *109*, D02S04. <https://doi.org/10.1029/2002JD003067>
- Majumder, C. A. H., Yuen, D. A., Sevre, E. O., Boggs, J. M., & Bergeron, S. Y. (2002). Finite Prandtl number 2-D convection at high Rayleigh numbers. *Visual Geosciences*, *7*(1), 1–53. <https://doi.org/10.1007/s10069-002-0004-4>
- Mertens, C. J., Mlynczak, M. G., López-Puertas, M., Wintersteiner, P. P., Picard, R. H., Winick, J. R., et al. (2001). Retrieval of mesospheric and lower thermospheric kinetic temperature from measurements of CO 215 μm Earth Limb Emission under non-LTE conditions. *Geophysical Research Letters*, *28*(7), 1391–1394. <https://doi.org/10.1029/2000GL012189>
- Miles, J. W., & Howard, L. N. (1964). Note on a heterogeneous shear flow. *Journal of Fluid Mechanics*, *20*(02), 331. <https://doi.org/10.1017/s0022112064001252>

- Nozawa, S., Kawahara, T. D., Saito, N., Hall, C. M., Tsuda, T. T., Kawabata, T., et al. (2014). Variations of the neutral temperature and sodium density between 80 and 107 km above Tromsø during the winter of 2010–2011 by a new solid-state sodium lidar. *Journal of Geophysical Research: Space Physics*, *119*, 441–451. <https://doi.org/10.1002/2013JA019520>
- Palmer, T. L., Fritts, D. C., & Andreassen, Ø. (1996). Evolution and breakdown of Kelvin–Helmholtz billows in stratified compressible flows. Part II: Instability structure, evolution, and energetics. *Journal of the Atmospheric Sciences*, *53*(22), 3192–3212. [https://doi.org/10.1175/1520-0469\(1996\)053<3192:eabokb>2.0.co;2](https://doi.org/10.1175/1520-0469(1996)053<3192:eabokb>2.0.co;2)
- Palmer, T. L., Fritts, D. C., Andreassen, Ø., & Lie, I. (1994). Three-dimensional evolution of Kelvin–Helmholtz billows in stratified compressible flow. *Geophysical Research Letters*, *21*(21), 2287–2290. <https://doi.org/10.1029/94GL01714>
- Peltier, W. R., & Caulfield, C. P. (2003). Mixing efficiency in stratified shear flows. *Annual Review of Fluid Mechanics*, *35*(1), 135–167. <https://doi.org/10.1146/annurev.fluid.35.101101.161144>
- Peterson, A. W. (1979). Airglow events visible to the naked eye. *Applied Optics*, *18*(20), 3390. <https://doi.org/10.1364/ao.18.003390>
- Pfrommer, T., Hickson, P., & She, C.-Y. (2009). A large-aperture sodium fluorescence lidar with very high resolution for mesopause dynamics and adaptive optics studies. *Geophysical Research Letters*, *36*, L15831. <https://doi.org/10.1029/2009GL038802>
- Qiu, S., Soon, W., Xue, X., Li, T., Wang, W., Jia, M., et al. (2018). Sudden sodium layers: Their appearance and disappearance. *Journal of Geophysical Research: Space Physics*, *123*, 5102–5118. <https://doi.org/10.1029/2017JA024883>
- Qiu, S., Tang, Y., Jia, M., Xue, X., Dou, X., Li, T., & Wang, Y. (2016). A review of latitudinal characteristics of sporadic sodium layers, including new results from the Chinese Meridian Project. *Earth-Science Reviews*, *162*, 83–106. <https://doi.org/10.1016/j.earscirev.2016.07.004>
- Qiu, X. L., & Tong, P. (2001). Onset of coherent oscillations in turbulent Rayleigh–Bénard convection. *Physical Review Letters*, *87*, 094501. <https://doi.org/10.1103/PhysRevLett.87.094501>
- Rahmani, M., Lawrence, G. A., & Seymour, B. R. (2014). The effect of Reynolds number on mixing in Kelvin–Helmholtz billows. *Journal of Fluid Mechanics*, *759*, 612–641. <https://doi.org/10.1017/jfm.2014.588>
- Rahmani, M., Seymour, B. R., & Lawrence, G. A. (2016). The effect of Prandtl number on mixing in low Reynolds number Kelvin–Helmholtz billows. *Physics of Fluids*, *28*(5), 054107. <https://doi.org/10.1063/1.4949267>
- Raizada, S., Tepley, C. A., Zhou, Q., Sarkhel, S., Mathews, J. D., Aponte, N. A., et al. (2015). Dependence of mesospheric Na and Fe distributions on electron density at Arecibo. *Earth, Planets and Space*, *67*(1), 146. <https://doi.org/10.1186/s40623-015-0322-z>
- Richardson, L. F. (1920). The supply of energy from and to atmospheric eddies. *Proceedings of the Royal Society A: Mathematical, Physical and Engineering Sciences*, *97*(686), 354–373. <https://doi.org/10.1098/rspa.1920.0039>
- Sarkhel, S., Mathews, J. D., Raizada, S., Sekar, R., Chakrabarty, D., Guharay, A., et al. (2015a). A case study on occurrence of an unusual structure in the sodium layer over Gadanki, India. *Earth, Planets and Space*, *67*, 19. <https://doi.org/10.1186/s40623-015-0183-5>
- Sarkhel, S., Mathews, J. D., Raizada, S., Sekar, R., Chakrabarty, D., Guharay, A., et al. (2015b). Erratum to: A case study on occurrence of an unusual structure in the sodium layer over Gadanki, India. *Earth, Planets and Space*, *67*, 145. <https://doi.org/10.1186/s40623-015-0276-1>
- Sarkhel, S., Mondal, S., Sekar, R., Chakrabarty, D., & Sridharan, S. (2019). A review on the upper atmospheric sodium observations from India: Insights. *Advances in Space Research*. <https://doi.org/10.1016/j.asr.2019.02.019>
- Sarkhel, S., Raizada, S., Mathews, J. D., Smith, S., Tepley, C. A., Rivera, F. J., & Gonzalez, S. A. (2012). Identification of large-scale billow-like structure in the neutral sodium layer over Arecibo. *Journal of Geophysical Research*, *117*, A10301. <https://doi.org/10.1029/2012JA017891>
- Sarkhel, S., Sekar, R., Chakrabarty, D., & Guharay, A. (2012). Investigation on mesospheric gravity waves over Indian low latitude stations using sodium airglow observations and a few case studies based on thermal and wind structures. *Journal of Atmospheric and Solar-Terrestrial Physics*, *86*, 41–50. <https://doi.org/10.1016/j.jastp.2012.06.008>
- Sarkhel, S., Sekar, R., Chakrabarty, D., Narayanan, R., & Sridharan, S. (2009). Simultaneous sodium airglow and lidar measurements over India: A case study. *Journal of Geophysical Research*, *114*, A10317. <https://doi.org/10.1029/2009JA014379>
- Sarkhel, S., Sekar, R., Chakrabarty, D., & Sridharan, S. (2010). A case study on the possible altitude-dependent effects of collisions on sodium airglow emission. *Journal of Geophysical Research*, *115*, A10306. <https://doi.org/10.1029/2010JA015251>
- Slipher, V. M. (1929). Emission in the spectrum of the light of the night sky. *Publications of the Astronomical Society of the Pacific*, *41*, 262–263.
- Sridharan, S., Prasanth, P. V., Kumar, Y. B., Ramkumar, G., Sathishkumar, S., & Raghunath, K. (2009). Observations of peculiar sporadic sodium structures and their relation with wind variations. *Journal of Atmospheric and Solar-Terrestrial Physics*, *71*(5), 575–582. <https://doi.org/10.1016/j.jastp.2008.12.002>
- Strobel, D. F. (1989). Constraints on gravity wave induced diffusion in the middle atmosphere. *Pure and Applied Geophysics*, *130*, 533. <https://doi.org/10.1007/BF00874473>
- Strobel, D. F., Apruzese, J. P., & Schoeberl, M. R. (1985). Energy balance constraints on gravity wave induced eddy diffusion in the mesosphere and lower thermosphere. *Journal of Geophysical Research*, *90*(D7), 13067. <https://doi.org/10.1029/JD090id07p13067>
- Strobel, D. F., Summers, M. E., Bevilacqua, R. M., DeLand, M. T., & Allen, M. (1987). Vertical constituent transport in the mesosphere. *Journal of Geophysical Research*, *92*(D6), 6691–6698. <https://doi.org/10.1029/JD092id06p06691>
- Takahashi, T., Nozawa, S., Tsutsumi, M., Hall, C., Suzuki, S., Tsuda, T. T., et al. (2014). A case study of gravity wave dissipation in the polar MLT region using sodium LIDAR and radar data. *Annales Geophysicae*, *32*(10), 1195–1205. <https://doi.org/10.5194/angeo-32-1195-2014>
- Taylor, M. J., & Hapgood, M. A. (1990). On the origin of ripple-type wave structure in the OH nightglow emission. *Planetary and Space Science*, *38*(11), 1421–1430. [https://doi.org/10.1016/0032-0633\(90\)90117-9](https://doi.org/10.1016/0032-0633(90)90117-9)
- Taylor, M. J., & Hill, M. J. (1991). Near infrared imaging of hydroxyl wave structure over an ocean site at low latitudes. *Geophysical Research Letters*, *18*(7), 1333–1336. <https://doi.org/10.1029/91GL01299>
- Taylor, M. J., Pendleton, W. R., Clark, S., Takahashi, H., Gobbi, D., & Goldberg, R. A. (1997). Image measurements of short-period gravity waves at equatorial latitudes. *Journal of Geophysical Research*, *102*(D22), 26,283–26,299. <https://doi.org/10.1029/96JD03515>
- Thorpe, S. A. (1968). A method of producing a shear flow in a stratified fluid. *Journal of Fluid Mechanics*, *32*(04), 693–704. <https://doi.org/10.1017/s0022112068000972>
- Thorpe, S. A. (1973). Experiments on instability and turbulence in a stratified shear flow. *Journal of Fluid Mechanics*, *61*(04), 731–751. <https://doi.org/10.1017/s0022112073000911>
- Thorpe, S. A. (2005). *The turbulent ocean*. Cambridge: Cambridge University Press.
- Tsuda, T. T., Nozawa, S., Kawahara, T. D., Kawabata, T., Saito, N., Wada, S., et al. (2011). Fine structure of sporadic sodium layer observed with a sodium lidar at Tromsø, Norway. *Geophysical Research Letters*, *38*, L18102. <https://doi.org/10.1029/2011GL048685>

- Tsuda, T. T., Nozawa, S., Kawahara, T. D., Kawabata, T., Saito, N., Wada, S., et al. (2015). A sporadic sodium layer event detected with five-directional lidar and simultaneous wind, electron density, and electric field observation at Tromsø, Norway. *Geophysical Research Letters*, *42*, 9190–9196. <https://doi.org/10.1002/2015GL066411>
- Werne, J., & Fritts, D. C. (1999). Stratified shear turbulence: Evolution and statistics. *Geophysical Research Letters*, *26*(4), 439–442. <https://doi.org/10.1029/1999GL900022>
- Xu, J., & Smith, A. K. (2003). Perturbations of the sodium layer: Controlled by chemistry or dynamics? *Geophysical Research Letters*, *30*(20), 2056. <https://doi.org/10.1029/2003GL018040>
- Zografos, A. I., Martin, W. A., & Sunderland, J. E. (1987). Equations of properties as a function of temperature for seven fluids. *Computer Methods in Applied Mechanics and Engineering*, *61*(2), 177–187. [https://doi.org/10.1016/0045-7825\(87\)90003-x](https://doi.org/10.1016/0045-7825(87)90003-x)